FIXED-FREE BEAM DYNAMICS PREDICTION FOR THIN RIB MACHINING BY RCSA

Andrew Honeycutt, and Tony L. Schmitz
Department of Mechanical Engineering and Engineering Science
University of North Carolina at Charlotte, Charlotte, NC

INTRODUCTION

It is common practice to produce monolithic metallic components with thin ribs from solid billets by machining (subtractive manufacturing). This enables complex parts with high strength-to-weight ratio to be produced without significant assembly time and cost. Application domains range from aerospace structures to laptop cases. With the recent advances in metal additive manufacturing, it is also possible to produce near net shape parts that require only minimal machining to provide the desired surface finish and dimensional accuracy. This is particularly attractive for titanium alloys due to their high material cost and low machinability. The inherent challenge with this hybrid (i.e., combined additive and subtractive) approach is machining flexible parts. The low dynamic stiffness of the thin, near net shape ribs limits both machining stability (i.e., chatter can occur) and part accuracy (via the surface location errors that can arise from forced vibrations) [1].

In prior work, finite element analysis has been the primary tool to model and predict the thin rib dynamics and, in many cases, the change in the rib dynamics as material is removed [2-20]. In this paper, an analytical approaches is presented to describe the stiffness and natural frequency of fixed-free beams, as well as the change in stiffness and natural frequency as material is removed by milling. The specific challenge of near net shape machining, where an initially thin rib is machined to produce a thinner rib, is addressed. Fixed-free beams with stepped profiles are used to represent the thin ribs geometries and subsequent material removal.

ANALYTICAL MODEL

Receptance coupling substructure analysis (RCSA) is a frequency domain, analytical procedure used to couple component receptances in order to predict the assembly receptances [21-22]. In this work, the free-free receptances for the machined section of a beam were rigidly coupled to the remaining (unmachined) fixed-free section; see Fig. 1. Using rigid compatibility and equilibrium conditions, the assembly direct receptances, $H_{11} = \frac{Y_1}{F_1}$ and $H_{22} = \frac{Y_2}{F_2}$, at assembly coordinates Y_1 and Y_2 are written as a function of the component receptances at coordinates 1, $2a$, and $2b$; see [21] for the derivation. The required direct and cross receptances for the free-free (coordinates 1 and $2a$) and fixed-free (coordinate $2b$) components are:

- $h_{11} = \frac{y_1}{f_1}$, $h_{12a} = \frac{y_1}{f_{2a}}$, $h_{2a1} = \frac{y_{2a}}{f_1}$, $h_{2a2a} = \frac{y_{2a}}{f_{2a}}$, and $h_{2b2b} = \frac{y_{2b}}{f_{2b}}$, where y_i is the component displacement and f_j is the (internal) component force
- $l_{11} = \frac{y_1}{m_1}$, $l_{12a} = \frac{y_1}{m_{2a}}$, $l_{2a1} = \frac{y_{2a}}{m_1}$, $l_{2a2a} = \frac{y_{2a}}{m_{2a}}$, and $l_{2b2b} = \frac{y_{2b}}{m_{2b}}$, where m_j is the (internal) component moment
- $n_{11} = \frac{\theta_1}{f_1}$, $n_{12a} = \frac{\theta_1}{f_{2a}}$, $n_{2a1} = \frac{\theta_{2a}}{f_1}$, $n_{2a2a} = \frac{\theta_{2a}}{f_{2a}}$, and $n_{2b2b} = \frac{\theta_{2b}}{f_{2b}}$, where θ_i is the component rotation
- $p_{11} = \frac{\theta_1}{m_1}$, $p_{12a} = \frac{\theta_1}{m_{2a}}$, $p_{2a1} = \frac{\theta_{2a}}{m_1}$, $h_{2a2a} = \frac{\theta_{2a}}{m_{2a}}$, and $p_{2b2b} = \frac{\theta_{2b}}{m_{2b}}$.

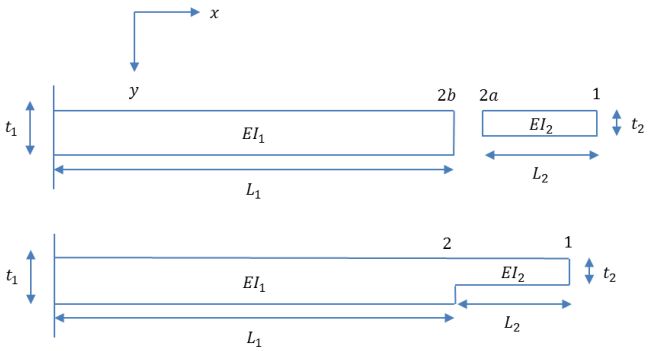

Figure 1. Beam model for RCSA. (Top) The two components and associated coordinates (1 and $2a$ for the free-free component and $2b$ for the fixed-free component) are identified. (Bottom) The assembly and associated coordinates (1 and 2) are shown.

The assembly receptances are provided in Eqs. 1 and 2 [21].

$$\begin{bmatrix} H_{11} & L_{11} \\ N_{11} & P_{11} \end{bmatrix} = \begin{bmatrix} h_{11} & l_{11} \\ n_{11} & p_{11} \end{bmatrix} - \begin{bmatrix} h_{12a} & l_{12a} \\ n_{12a} & p_{12a} \end{bmatrix} \left(\begin{bmatrix} h_{2a2a} & l_{2a2a} \\ n_{2a2a} & p_{2a2a} \end{bmatrix} + \begin{bmatrix} h_{2b2b} & l_{2b2b} \\ n_{2b2b} & p_{2b2b} \end{bmatrix} \right)^{-1} \begin{bmatrix} h_{2a1} & l_{2a1} \\ n_{2a1} & p_{2a1} \end{bmatrix} \quad (1)$$

$$\begin{bmatrix} H_{22} & L_{22} \\ N_{22} & P_{22} \end{bmatrix} = \begin{bmatrix} h_{2a2a} & l_{2a2a} \\ n_{2a2a} & p_{2a2a} \end{bmatrix} - \begin{bmatrix} h_{2a2a} & l_{2a2a} \\ n_{2a2a} & p_{2a2a} \end{bmatrix} \left(\begin{bmatrix} h_{2a2a} & l_{2a2a} \\ n_{2a2a} & p_{2a2a} \end{bmatrix} + \begin{bmatrix} h_{2b2b} & l_{2b2b} \\ n_{2b2b} & p_{2b2b} \end{bmatrix} \right)^{-1} \begin{bmatrix} h_{2a2a} & l_{2a2a} \\ n_{2a2a} & p_{2a2a} \end{bmatrix} \quad (2)$$

The component receptances can be obtained from measurements or models. Two modeling options are the Euler-Bernoulli and Timoshenko beams. In this work, the one-dimensional Timoshenko beam model was implemented to find the free-free receptances. This requires a numerical solution of the partial differential equation displayed in Eq. 3 [23-24], where $\hat{k}$ is a shape factor that depends on the beam's cross section [25]. To determine the required fixed-free receptances for the L_1 section component, the free-free receptances for this component (obtained from Eq. 19) were rigidly coupled to a rigid boundary (i.e., zero receptances). Equation 1 was also applied for this sub-step, where the $2b$ coordinate was assigned to the rigid boundary and the 1 and $2a$ coordinates to the L_1 section component.

$$\left(\frac{\partial^2 y}{\partial t^2} + \frac{EI}{\rho A} \frac{\partial^4 y}{\partial x^4} \right) + \left(\frac{\rho I}{\hat{k} AG} \frac{\partial^4 y}{\partial t^4} + \frac{EI}{\hat{k} AG} \frac{\partial^4 y}{\partial x^2 \partial t^2} \right) - \left(\frac{I}{A} \frac{\partial^4 y}{\partial x^2 \partial t^2} \right) = 0 \quad (3)$$

Table 1. Comparison of FE and RCSA natural frequency predictions.

L_1 (mm)	L_2 (mm)	FE f_n (Hz)	Analytical f_n (Hz)	% difference
150	0	217.96	217.87	0.04
146	4	221.79	221.70	0.04
142	8	225.51	225.42	0.04
132	18	234.28	234.19	0.04
122	28	242.03	241.96	0.03
100	50	253.20	253.37	-0.07
75	75	248.22	249.26	-0.42
50	100	219.84	221.82	-0.90
25	125	180.46	182.63	-1.20
10	140	157.53	159.54	-1.28
0	150	145.39	145.34	0.03

To provide a numerical validation of the analytical coupling approach, comparisons between the RCSA predictions and ANSYS finite element calculations were completed. Multiple beam geometries were tested where the beam thickness was reduced from 6 mm (t_1) to 4 mm (t_2) over a varying length, L_2. In each case, the natural frequency and modal stiffness were extracted by peak picking from the direct receptances. Natural frequency results are presented in Table 1 and Fig. 2, where the steel beam's elastic modulus was 200 GPa, its width was 20 mm, Poisson's ratio was 0.3, and the density was 7800 kg/m^3.

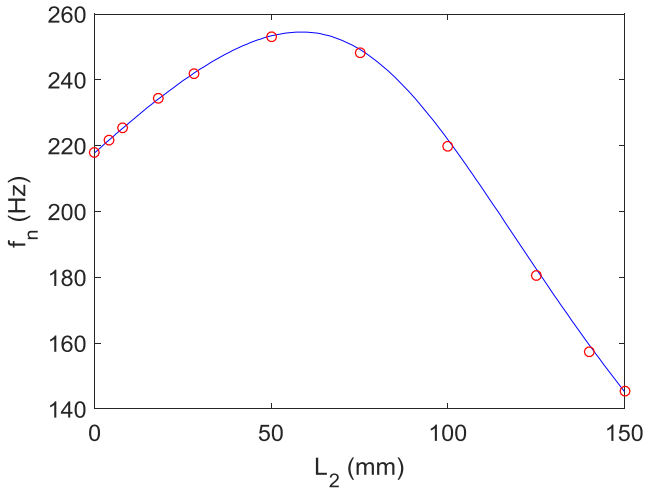

Figure 2. Graphical comparison of FE (circles) and RCSA (line) natural frequency predictions.

The k_1 stiffness results (from H_{11}) are presented in Table 2 and Fig. 3. The k_2 stiffness results (from H_{22}) are provided in Table 3 and Fig. 4.

Table 2. Comparison of FE and RCSA k_1 stiffness predictions.

L_1 (mm)	L_2 (mm)	FE k_1 (N/m)	Analytical k_1 (N/m)	% difference
150	0	6.59×10^4	6.58×10^4	0.24
146	4	6.61×10^4	6.59×10^4	0.24
142	8	6.62×10^4	6.60×10^4	0.24
132	18	6.63×10^4	6.62×10^4	0.22
122	28	6.61×10^4	6.60×10^4	0.13
100	50	6.24×10^4	6.26×10^4	-0.33
75	75	5.17×10^4	5.22×10^4	-1.12
50	100	3.84×10^4	3.91×10^4	-1.63
25	125	2.73×10^4	2.78×10^4	-1.84
10	140	2.21×10^4	2.25×10^4	-1.88
0	150	1.954×10^4	1.95×10^4	0.12

EXPERIMENTAL SETUP

Receptance measurements were completed using a modal hammer (PCB 086C04) to excite the beam and a laser vibrometer (Polytec OFV 5000 controller/OFV 534 laser head) to measure the velocity; see Fig. 5. The direct receptance measurements were performed at the aluminum beam's free end and at the change in thickness. The length of the reduced thickness section was changed by machining, where a 12.7 mm diameter three-flute solid carbide endmill

(approximately 100 mm stickout length) was used (0.1 mm/tooth, 3900 rpm). The beam thickness was removed in 10 mm axial steps with a final radial depth of 1 mm. The beam width was 44.96 mm. Measurements were performed after each machining pass.

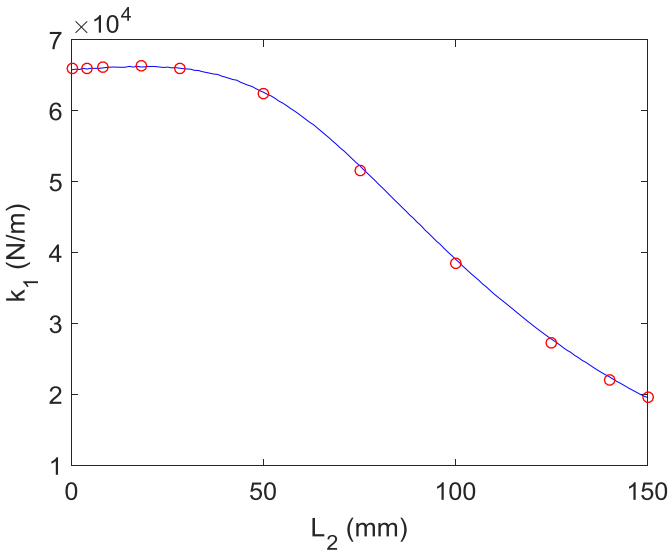

Figure 3. Graphical comparison of FE (circles) and RCSA (line) k_1 stiffness predictions.

Table 3. Comparison of FE and Raleigh method k_2 stiffness predictions.

L_1 (mm)	L_2 (mm)	FE k_2 (N/m)	Analytical k_2 (N/m)	% difference
150	0	-	-	-
146	4	7.12×10^4	7.10×10^4	0.24
142	8	7.70×10^4	7.68×10^4	0.25
132	18	9.49×10^4	9.46×10^4	0.26
122	28	1.19×10^5	1.19×10^5	0.28
100	50	2.23×10^5	2.22×10^5	0.50
75	75	6.45×10^5	6.37×10^5	1.27
50	100	3.60×10^6	3.52×10^6	2.21
25	125	7.19×10^7	6.99×10^7	2.78
10	140	3.25×10^9	3.15×10^9	3.12
0	150	-	-	-

RESULTS

A comparison between experiments and RCSA receptances was completed for the fundamental bending mode of the aluminum beam displayed in Fig. 5. For the RCSA beams models, the elastic modulus was 69 GPa, Poisson's ratio was 0.33, and the density was 2700 kg/m^3. The natural frequency results are displayed in Table 4 and Fig. 6. The k_1 stiffness results are presented in Table 5 and Fig. 7. The k_2 stiffness results are shown in Table 6 and Fig. 8. In all cases, the parameters were extracted by modal fitting.

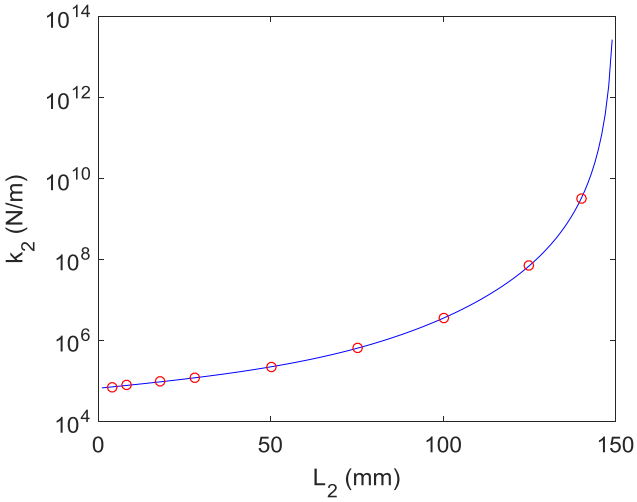

Figure 4. Graphical comparison of FE (circles) and RCSA (line) k_2 stiffness predictions (semilog scale).

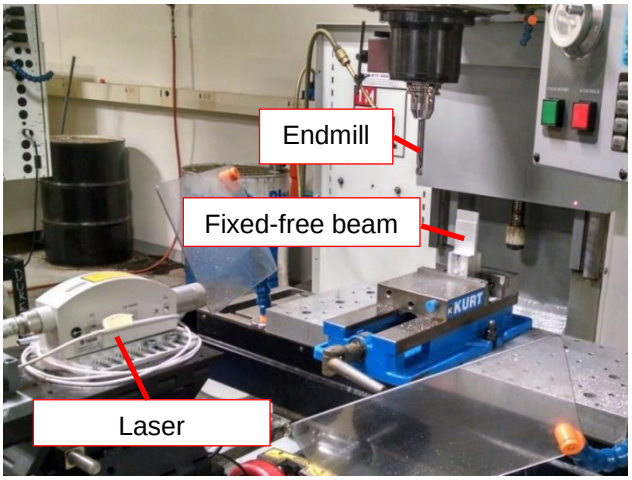

Figure 5. Experimental setup. The fixed-free aluminum beam was mounted in a vise which was clamped to the machine table. The laser vibrometer was used to measure the beam response due to a force impact (applied by a modal hammer).

Table 4. Comparison of experiments and RCSA predictions for natural frequency.

L_1 (mm)	L_2 (mm)	Experiment f_n (Hz)	RCSA f_n (Hz)	% difference
80	0	749	762.4	-1.78
70	10	776	790.39	-1.85
60	20	793	810.25	-2.18
50	30	804	820.04	-2.00
40	40	800	816.27	-2.03
30	50	781	795.15	-1.81

20	60	743	755.49	-1.68
10	70	691	700.45	-1.37
0	80	630	636.14	-0.97

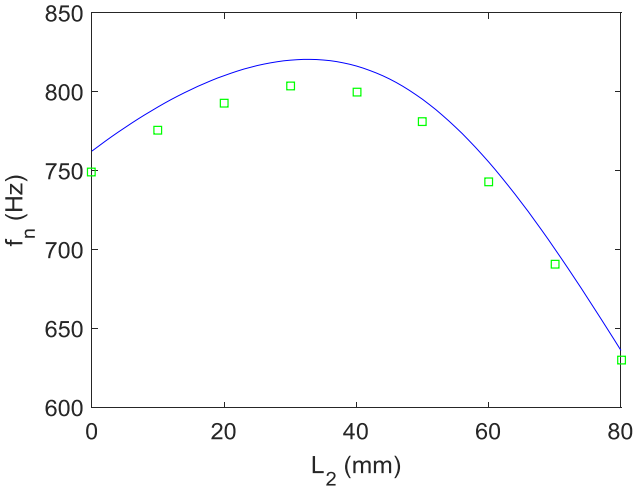

Figure 6. Graphical comparison of experiments (squares) and RCSA (line) natural frequency predictions.

Table 5. Comparison of experiments and RCSA predictions for stiffness k_1.

L_1 (mm)	L_2 (mm)	Exp. k_1 (N/m)	RCSA k_1 (N/m)	% difference
80	0	3.68×10^5	3.34×10^5	9.27
70	10	3.35×10^5	3.35×10^5	0.04
60	20	3.51×10^5	3.33×10^5	5.12
50	30	3.30×10^5	3.25×10^5	1.38
40	40	3.33×10^5	3.10×10^5	6.99
30	50	2.89×10^5	2.86×10^5	1.03
20	60	2.97×10^5	2.57×10^5	13.6
10	70	2.30×10^5	2.25×10^5	2.14
0	80	1.93×10^5	1.94×10^5	-0.40

Table 6. Comparison of experiments and RCSA predictions for stiffness k_2.

L_1 (mm)	L_2 (mm)	Exp. k_2 (N/m)	RCSA k_2 (N/m)	% difference
80	0	-	-	-
70	10	6.07×10^5	4.87×10^5	19.8
60	20	9.02×10^5	7.69×10^5	14.7
50	30	1.72×10^6	1.38×10^6	20.0
40	40	3.92×10^6	2.97×10^6	24.2
30	50	1.46×10^7	8.68×10^6	40.6
20	60	6.21×10^7	4.26×10^7	31.5
10	70	2.24×10^8	6.80×10^8	-203.5
0	80	-	-	-

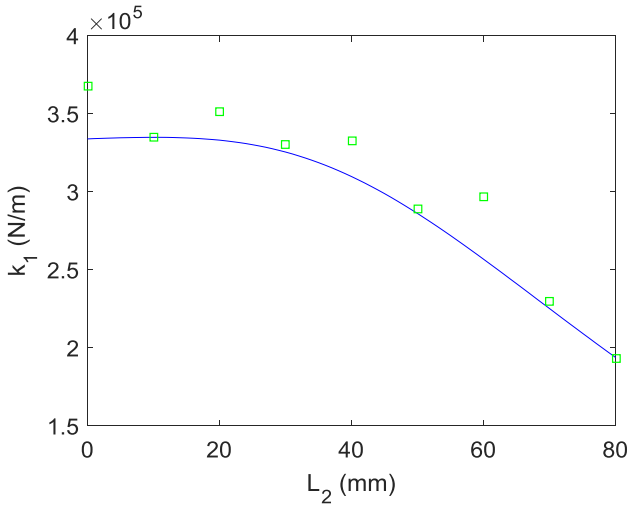

Figure 7. Graphical comparison of experiments (squares) and RCSA (line) k_1 stiffness predictions.

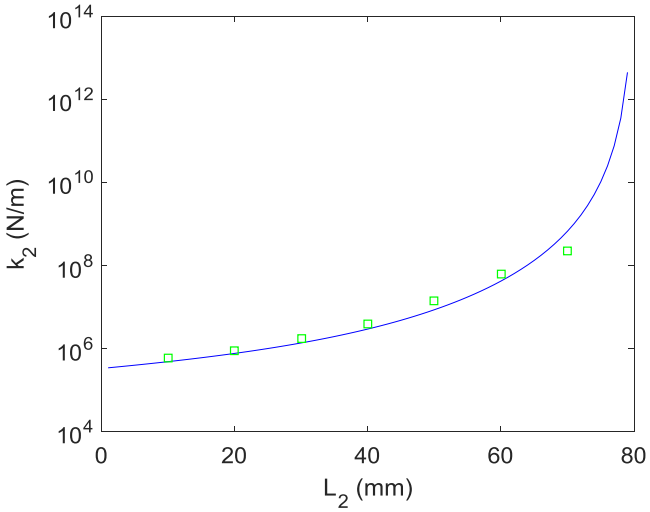

Figure 8. Graphical comparison of experiments (squares) and RCSA (line) k_2 stiffness predictions (semilog scale).

CONCLUSIONS

An analytical approach was presented for predicting thin rib, fixed-free beam dynamics with varying geometries. The method was based on receptance coupling substructure analysis (RCSA). Comparison with finite element calculations showed good agreement with the RCSA approach using the Timoshenko beam model to predict the component receptances.

Experiments were conducted to compare measured fixed-free beam receptances to RCSA predictions. An aluminum beam was machined between receptance measurements to change the thickness. The measured and predicted natural

frequencies agreed with an average percent difference of -1.74% for the nine beam profiles. The measured and predicted stiffness values for the fundamental bending mode at the beam's free end agreed with an average percent difference of 4.35% for the nine beam profiles. The measured and predicted stiffness values for the fundamental bending mode at the location of the beam's change in thickness agreed with an average percent difference of -7.53% for the seven beam profiles with a step change in thickness (i.e., the initial and final thin ribs are excluded from this analysis because they both have a uniform thickness).

In addition to the natural frequency and stiffness values, the dimensionless viscous damping ratios, ζ, were extracted from the measured direct receptances. These values are critical because first principle techniques for damping prediction are not available and the damping must, therefore, be included by the modeler based on experience or measurements. The results for the aluminum beam are displayed in Fig. 8 for all nine geometries; damping ratios were extracted from direct receptance measurements at both the free end and thickness change location. The average damping ratio is 0.28% with a standard deviation of 0.04%. The low damping for monolithic structures exacerbates the challenges associated with machining thin, near net shape ribs to produce the final thinner geometries.

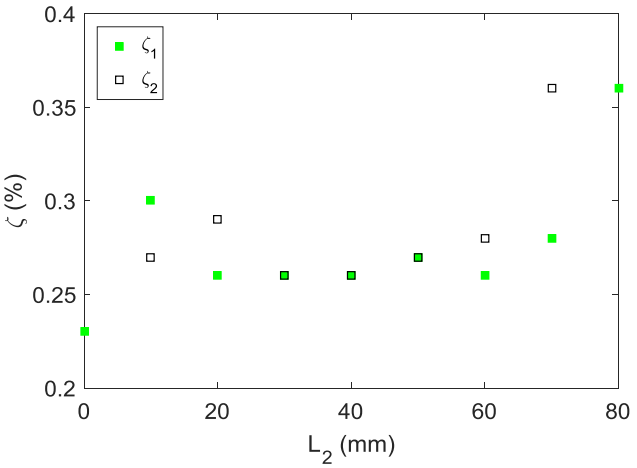

Figure 8. Experimental damping ratio values from direct receptances at the beam's free end, ζ_1, and at the location of the step change in thickness, ζ_2.

ACKNOWLEDGEMENTS

The authors thank Dr. John Ziegert for helpful discussions. They also gratefully acknowledge partial financial support from the National Science Foundation (Grant No. CMMI-1561221).

REFERENCES

[1] Schmitz, T. and Smith, K.S., 2009, Machining Dynamics: Frequency Response to Improved Productivity, Springer, New York, NY.

[2] Budak, E., Altintas, Y., 1995, Modeling and avoidance of static form errors in peripheral milling of plates, International Journal of Machine Tools & Manufacture, 35: 459-476.

[3] Tlusty, J., Smith, S., and Winfough, W., 1996, Techniques for the use of long slender end mills in high-speed milling, Annals of the CIRP, 45/1: 393-396.

[4] Smith, S. and Dvorak, D., 1998, Tool path strategies for high speed milling aluminum workpieces with thin webs, Mechatronics, 8: 291-300.

[5] Ning, H., Zhigang, W., Chengyu, J., and Bing, Z., 2003, Finite element method analysis and control stratagem for machining deformation of thin-walled components, Journal of Materials Processing Technology, 139: 332-336.

[6] Ratchev, S., Nikov, S., and Moualek, I., 2004, Material removal simulation of peripheral milling of thin wall low-rigidity structures using FEA, Advances in Engineering Software, 35: 481-491.

[7] Ratchev, S., Liu, S., Huang, W., and Becker, A.A., 2004, Milling error prediction and compensation in machining of low-rigidity parts, International Journal of Machine Tools & Manufacture, 44: 1629-1641.

[8] Bravo, U., Altuzarra, O., López de Lacalle, L.N., Sánchez, J.A., and Campa, F.J., 2005, Stability limits of milling considering the flexibility of the workpiece and the machine, International Journal of Machine Tools & Manufacture, 45: 1669-1680.

[9] Ratchev, S., Liu, S., and Becker, A.A., 2005, Error compensation strategy in milling flexible thin-wall parts, Journal of Materials Processing Technology, 162-163: 673-681.

[10] Thevenot, V., Arnaud, L., Dessein, G., and Cazenave-Larroche, G., 2006, Influence of material removal on the dynamic behavior of thin-walled structures in peripheral milling, Machining Science and Technology, 10/3: 275-287.

[11] Mañé, I., Gagnol, V., Bouzgarrou, B.C., and Ray, P., 2008, Stability-based spindle speed control during flexible workpiece high-speed milling, International Journal of Machine Tools & Manufacture, 48: 184-194.

[12] Rai, J.K. and Xirouchakis, P., 2008, Finite element method based machining simulation environment for analyzing part errors induced during milling of thin-walled components, International Journal of Machine Tools & Manufacture, 48: 629-643.

[13] Seguy, S., Dessein, G., and Arnaud, L., 2008, Surface roughness variation of thin wall milling, related to modal interactions, International Journal of Machine Tools & Manufacture, 48: 261-274.
[14] Adetoro, O.B., Wen, P.H., Sim, W.M., and Vepa, R., 2009, Stability lobes prediction in thin wall machining, Proceedings of the World Congress on Engineering 2009 Vol I, WCE 2009, July 1-3, 2009, London, UK.
[15] Chen, W., Xue, J., Tang, D., Chen, H., and Qu, S., 2009, Deformation prediction and error compensation in multilayer milling processes for thin-walled parts, International Journal of Machine Tools & Manufacture, 49: 859-864.
[16] Gang, L., 2009, Journal of Materials Processing Technology, Study on deformation of titanium thin-walled part in milling process, 209: 2788-2793.
[17] Arnaud, L., Gonzalo, O., Seguy, S., Jauregi, H., and Peigné, G., 2011, Simulation of low rigidity part machining applied to thin-walled structures, International Journal of Advanced Manufacturing Technology, 54: 479-488.
[18] Izamshah, R., Mo, J.P.T , and Ding, S., 2011, Hybrid deflection prediction on machining thin-wall monolithic aerospace components, Proc. IMechE Part B: Journal of Engineering Manufacture, 226: 592-605.
[19] Smith, S., Wilhelm, R., Dutterer, B., Cherukuri, H., and Goel, G., 2012, Sacrificial structure preforms for thin part machining, CIRP Annals - Manufacturing Technology, 61: 379-382.
[20] Polishetty, A., Goldberg, M., Littlefair, G., Puttaraju, M., and Patil, P., 2014, A preliminary assessment of machinability of titanium allow Ti 6Al 4V during thin wall machining using trochoidal milling, Procedia Engineering, 97: 357-364.
[21] Schmitz, T. and Smith, K.S., 2012, Mechanical Vibrations: Modeling and Measurement, Springer, New York, NY.
[22] Bishop, R.E.D., and Johnson, D.C., 1960, The Mechanics of Vibration, Cambridge University Press, Cambridge, UK.
[23] Weaver, Jr., W., Timoshenko, P., and Young, D., 1990, Vibration Problems in Engineering, 5th Ed., John Wiley and Sons, New York, NY.
[24] Schmitz, T. and Duncan, G.S., 2005, Three-component receptance coupling substructure analysis for tool point dynamics prediction, Journal of Manufacturing Science and Engineering, 127/4: 781-790.
[25] Hutchinson, J., 2001, Shear coefficients for Timoshenko beam theory, Journal of Applied Mechanics, 68: 87-92.